Human Molecular Genetics, 2013, Vol. 22, No. 20 **4164–4179**
doi:10.1093/hmg/ddt264
Advance Access published on June 6, 2013

Differentiation of epidermal keratinocytes is dependent on glucosylceramide:ceramide processing

Nicole Amen[1], Daniel Mathow[1], Mariona Rabionet[1,2], Roger Sandhoff[1,2], Lutz Langbein[3], Norbert Gretz[4], Carsten Jäckel[5], Hermann-Josef Gröne[1,*] and Richard Jennemann[1,*]

[1]Division of Cellular & Molecular Pathology, [2]Lipid Pathobiochemistry and [3]Genetics of Skin Carcinogenesis, German Cancer Research Center, D-69120 Heidelberg, Germany [4]Medical Research Center Mannheim, University of Heidelberg, Mannheim, Germany [5]Clinical Biochemistry, University Hospital Munich, LMU University Munich, Munich, Germany

Received February 12, 2013; Revised and Accepted June 3, 2013

Skin barrier function is primarily assigned to the outer epidermal layer, the *stratum corneum* (SC), mainly composed of corneocytes and lipid-enriched extracellular matrix. Epidermal ceramides (Cers) are essential barrier lipids, containing ultra-long-chain (ULC) fatty acids (FAs) with a unique ω-hydroxy group, which is necessary for binding to corneocyte proteins. In the SC, Cers are believed to derive from glucosylated intermediates, namely glucosylceramides (GlcCers), as surmised from human Gaucher's disease and related mouse models. Tamoxifen (TAM)-induced deletion of the endogenous GlcCer-synthesizing enzyme UDP-glucose:ceramide glucosyltransferase (UGCG) in keratin K14-positive cells resulted in epidermal GlcCer depletion. Although free extractable Cers were elevated in total epidermis and as well in SC, protein-bound Cers decreased significantly in *Ugcg*$^{f/fK14CreERT2}$ mice, indicating glucosylation to be required for regular Cer processing as well as arrangement and extrusion of lipid lamellae. The almost complete loss of protein-bound Cers led to a disruption of the water permeability barrier (WPB). UGCG-deficient mice developed an ichthyosis-like skin phenotype marked by impaired keratinocyte differentiation associated with delayed wound healing. Gene expression profiling of *Ugcg*-mutant skin revealed a subset of differentially expressed genes involved in lipid signaling and epidermal differentiation/proliferation, correlating to human skin diseases such as psoriasis and atopic dermatitis. Peroxisome proliferator-activated receptor beta/delta (PPARβ/δ), a Cer-sensitive transcription factor was identified as potential mediator of the altered gene sets.

INTRODUCTION

The skin permeability barrier primarily resides in the outermost anucleated layers of the epidermis, i.e. the *stratum corneum* (SC). This barrier, preventing dehydration, and serving as a protective sheath against mechanical insult and infection, is believed to derive from the interplay of proteins in the corneocyte membrane with lipids (1). Corneocytes are surrounded by a lipid-coated lamellar matrix composed of ceramides (Cers), cholesterol and free fatty acids (FAs) which occur in almost equimolar ratios and allow for the arrangement into lamellar sheets (1,2). Cers are synthesized in the endoplasmic reticulum (ER) and then translocated to the Golgi where UDP-activated glucose is added on the cytosolic surface by action of the enzyme UDP-glucose ceramide glucosyltransferase (UGCG) (3,4). The resulting glucosylceramides (GlcCers) are the dominant glycosphingolipids (GSLs) synthesized by keratinocytes (KCs) and comprise ca. 4% of the total lipid mass in the epidermis (5). The lipophilic anchor of epidermal GlcCers contains a unique ultra-long-chain (ULC) amide-linked FA with 28–36 carbon atoms (6). The ULC-FAs are typically ω-hydroxylated (ωh) to give the so-called OS class of GlcCers, accounting for an essential part of the skin barrier. GlcCers are thought to act as intracellular carriers of these strongly hydrophobic Cers and

*Correspondence to be addressed at: DKFZ-G130, INF 280, 69120 Heidelberg, Germany. Tel: +49 6221424350; Fax: +49 6221424352; Email: h.-j.groene@dkfz.de (H.-J.G.); Tel: +49 6221424356; Fax: +49 6221424352; Email: r.jennemann@dkfz.de (R.J.)

are a major component of lamellar bodies (LBs) (7–9). LBs fuse with the apical plasma membrane at the interface of the *stratum granulosum* (SG)–SC to exocytose their lamellar content, together with structural proteins, enzymes and antimicrobial peptides into the extracellular space (10,11). By the action of enzymes such as β-glucocerebrosidase and ceramidase, Cers and glucose as well as FAs and free sphingoid bases are released from GlcCer-precursors. The ωh-group of ULC-(Glc)Cers enables their esterification to an additional FA, predominantly linoleic acid (C18:2, ω-6), to give the EOS subclass of (Glc)Cers. Transesterification to proteins of the corneocyte membrane [i.e. involucrin (IVL), envoplakin (EVPL), periplakin (PPL) and loricrin (LOR)] leads to protein-bound Cers and to the formation of the cornified lipid envelope (12–15). EOS as well as protein-bound species including their corresponding GlcCer-precursors establish the extremely hydrophobic extracellular lipid lamellae of the SC and thereby the skin barrier (16,17).

An earlier study using mice with constitutive *Ugcg* deletion in the epidermis (*Ugcg*$^{f/fK14Cre}$ mice) highlighted the importance of Cer-glucosylation. Mutant mice lost the water permeability barrier (WPB) and died postnatally at day P5 (18). However, the exact molecular and cellular contribution of OS- and specifically protein-bound Cers for the built-up and stability of the WPB could not be determined (18). In addition, the differentiation and function of UGCG-deficient epidermis and its function in clinically relevant pathophysiologic states e.g. wound healing have not been elucidated.

We generated inducible *Ugcg*$^{f/fK14CreERT2}$ mice to circumvent the problem of early death experienced with *Ugcg*$^{f/fK14Cre}$ mice. Tamoxifen (TAM)-induced *Ugcg* gene deletion in basal layer KCs resulted in a significant decrease in epidermal GlcCers and, in contrast to newborn mice, to an almost complete loss of protein-bound Cers 3 weeks after initiation of TAM induction. Subsequent loss of epidermal differentiation and barrier homeostasis was evidenced by an increase in transepidermal water loss (TEWL) and pH as well as by KC hyperproliferation and disordered differentiation to give a severe ichthyosiform skin phenotype. Wound closure and reepithelialization was significantly delayed in mutant vs. control mice. The increase in Cers upon *Ugcg* deletion led to an increase of PPARß/δ and induction of potential target genes involved in epidermal proliferation and differentiation.

RESULTS

Ugcg$^{f/fK14CreERT2}$ mice lack epidermal GlcCers and protein-bound Cers upon TAM induction

To study the role of Cer-glucosylation in the epidermis of adult mice (Fig. 1A), TAM-inducible *Ugcg*$^{f/fK14CreERT2}$ mice were generated (Fig. 1B and Supplementary Material, Fig. S1). *Ugcg* gene deletion was identified by Southern blot analysis in all stratified epithelia, such as epidermis, tongue, esophagus and forestomach and in hair follicle outer root sheath KCs residing in the dermis (Fig. 1C). Epidermal sphingolipids (SLs) were investigated by thin layer chromatography (TLC) (Fig. 2A, A′, B) and quantitative mass spectrometry (MS) (Fig. 2C–F). Free extractable GlcCers were significantly reduced by ∼80% (Fig. 2A, A′, C), whereas free extractable Cers were found to be significantly increased (Fig. 2D) in UGCG-deficient epidermis compared with controls. Free Cers increased not only in epidermis but also in isolated SC as demonstrated for OS- and EOS-Cers. A similar elevation as in total epidermal extracts could be demonstrated by MS. Within the SMs, alpha-hydroxylated (AS) species were significantly decreased, instead the minor OS and EOS compounds were significantly elevated (Fig. 2E). EOS-SMs were predominantly esterified with linoleic acid which is apparently similar to EOS-Cers (Supplementary Material, Figs S2–4). A complete list of all measured SLs sorted by amide-linked FA chain length is provided in Supplementary Material, Table S4.

The highest reduction (by 82%) in the epidermis was observed for protein-bound Cers and the few protein-bound GlcCers (Fig. 2F), essential lipids for epidermal permeability barrier function. SC lipid lamellar organization, shown by Nile Red staining, displayed orderly structured lipid lamellae in controls, whereas in mutant mice the SC was interspersed with granular-like lipid aggregates within disordered lamellar sheets (Fig. 2G).

Lipid lamellae of LBs in *Ugcg*-mutant SC are discontinuous

Transmission electron micrographs of ventral skin sections evidenced normal oval-shaped LBs and lipid lamellae in the SC of control epidermis (Fig. 3A). Instead, in *Ugcg*-mutant skin LBs displayed an irregular tubular shape containing irregular lamellar lipid structures (Fig. 3B). In the extracellular space, lipid sheaths (deriving from LBs) were discontinuous in *Ugcg*$^{f/fK14CreERT2}$ mice when compared with controls (Fig. 3).

GlcCer depletion leads to hyperkeratosis and WPB breakdown alleviated by hair follicle stem cell-driven epidermal regeneration. *Ugcg*$^{f/fK14CreERT2}$ mice were easily distinguishable from controls in the third week of TAM induction (1 mg TAM/injection/week) displaying sticky fur, dark tail skin and pruritus (data not shown). Dry, flaky skin became visible at the end of the third induction week (Fig. 4A). A hyperstratified and hyperkeratotic mutant epidermis was observed (Fig. 4B) with a ∼5-fold increase in epidermal thickness (Fig. 4C). Significant weight loss of mutants was observed in parallel with increasing TEWL at the end of week 3 (Fig. 4D and E), indicating the onset of WPB disruption. GlcCer-deficient mice sufficiently compensated high epidermal water loss with increased water uptake from that time point on (Fig. 4F). In addition to the extremely high water evaporation from mutant skin, both a significant decrease in the body temperature (Fig. 4G) and weight loss occurred upon 6 h water deprivation (Supplementary Material Fig. S6a–e). Impaired barrier function was further indicated by significantly elevated SC pH (pH 6.1 *Ugcg*$^{f/fK14CreERT2}$ vs. pH 5.1 *Ugcg* controls) (Fig. 4H), which is an important regulator of SC cohesion and desquamation in healthy skin (19). TEWL, water uptake, body weight and Cre-activity were monitored over 3 months in order to investigate whether *Ugcg*-mutant skin recovered from WPB loss (Supplementary Material, Fig. S7a–d). TEWL and water uptake constantly decreased, but remained significantly elevated in *Ugcg* mutants when compared with controls. Cre-activity was demonstrated in the epidermis for all investigated time points (with highest intensity in the second and fourth week upon induction). However, the infundibulum lost positivity ∼8–10 weeks after TAM induction (Supplementary Material, Fig. S7d). Accordingly, hyperkeratosis

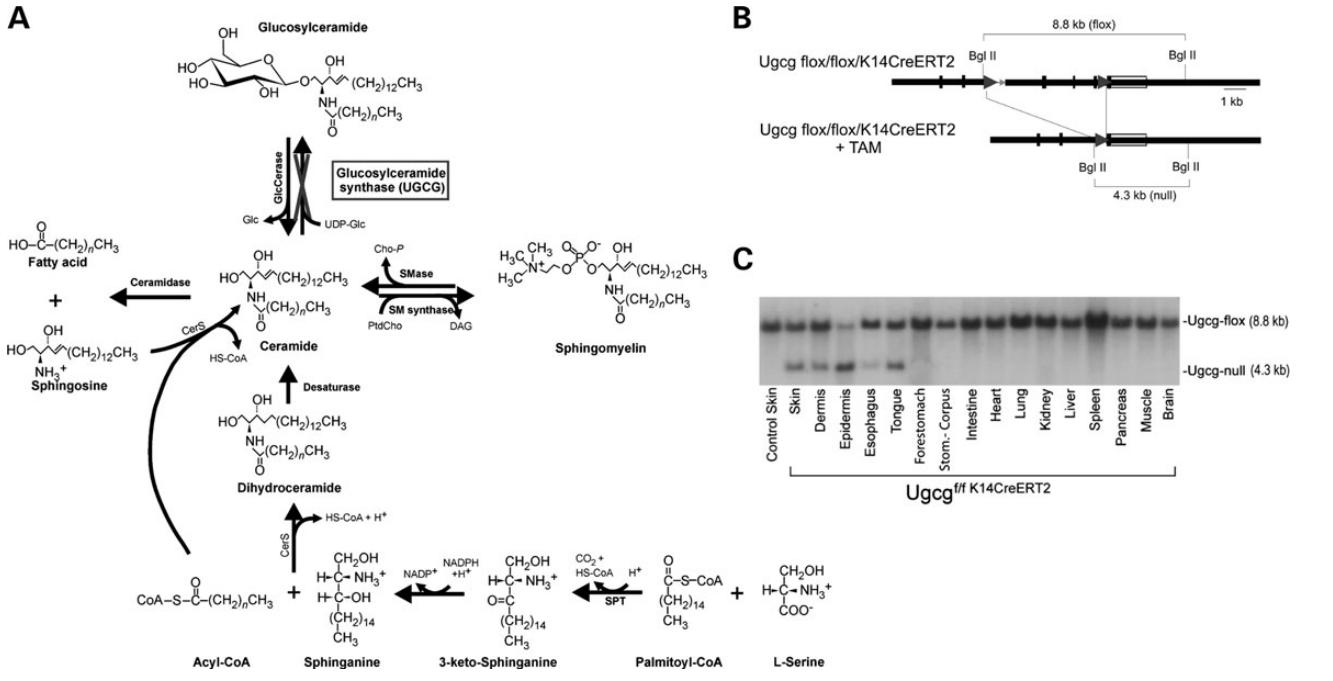

Figure 1. Generation of *Ugcg*$^{f/fK14CreERT2}$ mice. (**A**) Inhibition of glucosylceramide (GlcCer) biosynthesis in murine epidermis was achieved by deletion of glucosylceramide synthase (UGCG) specifically in keratin K14 expressing cells upon TAM-induced Cre-recombinase activation (**B**). (**C**) Tissue specificity of *Ugcg* gene recombination was confirmed by southern blot analysis. Besides skin, recombinations were detected in tongue, esophagus and forestomach. Positivity of the dermis resulted from K14-positive recombinant cells of epidermal appendages (e.g. hair follicle outer root sheath keratinocytes).

persisted in particular at locations with low hair follicle density, e.g. ear and paw, implying the action of K14-negative hair follicle stem cells in epidermal barrier restoration. Hyperproliferation was documented by an increased number of Ki67-positive cells in basal, para- and lower suprabasal layers of the epidermis (Supplementary Material, Fig. S8a, a′). Immune cell activation upon epidermal barrier loss resulted in an increase of dendritic cells/macrophages in dermis and lower epidermis of mutant mice (Supplementary Material, Fig. S8b, b′). However, no significant difference in granulocytes and mast cells was detected between both groups (Supplementary Material, Fig. S8c, c′).

Keratinocyte differentiation is disturbed

Epidermal differentiation is achieved by a complex signaling and remodeling process in which basal KCs migrate upwards and continuously differentiate until they go into stepwise apoptosis and finally shed off during desquamation (20). Immunofluorescence (IF) microscopy was used to characterize KC maturation. Keratin K14 was normally expressed in the basal layer KCs in control skin but was additionally present in all suprabasal layers of GlcCer-deficient skin, indicating abnormal KC differentiation (Fig. 5A). Keratin K10 was expressed in the differentiated KCs of the *stratum spinosum* (SS) and SG layers in control skin. In mutants, K10 was distributed in the normal manner, including the 5-fold multilayered epidermis (Fig. 5B). Keratin K6 was present in all viable epidermal layers in the mutant, but absent in control skin, reflecting the hyperproliferative state of GlcCer-deficient epidermis (Fig. 5C). The abnormal KC differentiation was further demonstrated by numerous nuclear remnants in SC layers of *Ugcg*-mutant skin (Fig. 5A–C, E, F). Altogether, the epidermis of *Ugcg* mutants appeared as a disorganized hyperproliferative layer.

To closer examine the epidermal integrity of mutant skin, junction proteins such as tight junctions (TJs) and desmosomes were investigated. TJ protein claudin 1 (CLDN1) and the desmosomal cadherins desmoglein 1 and 2 [DSG1/2; the antibody used labels both isoforms; (21)] were detectable in all viable epidermal layers in controls—with DSG2 in the basal and DSG1 in the suprabasal strata. The mutant skin showed a slightly weaker punctuate staining which was more concentrated at the cell margins of the large hyperproliferative cells and was practically absent in the basal layer (Fig. 5D and E) indicating a reduction of DSG2. Quantitative differences of CLDN1 and DSG1/2 were corroborated by western blotting in GlcCer-depleted epidermis (Fig. 6A), in accord with the leakiness of the epidermal junction barrier. Furthermore, the desmosomal catenin desmoplakin (DSP), was strongly expressed in all viable strata in mutant epidermis, demonstrated by its typical punctuate diffuse staining pattern in the basal and spinous layers, which was more concentrated at cell membranes in the upper layers (Fig. 5F). In addition to the leakiness of the SC lipid barrier, these results suggest deficient junction formation (CLDN1 and DSG2) to also contribute to the epidermal barrier loss.

Formation of the cornified envelope (CE) is delayed

The cornified envelope (CE) is formed during corneocyte maturation. Its formation relies to a major part on the synthesis and cross-linking of both structural proteins such as IVL and LOR with EVPL and small proline-rich proteins (SPRRPs) as well as lipids (20). The plasma membrane gets gradually replaced

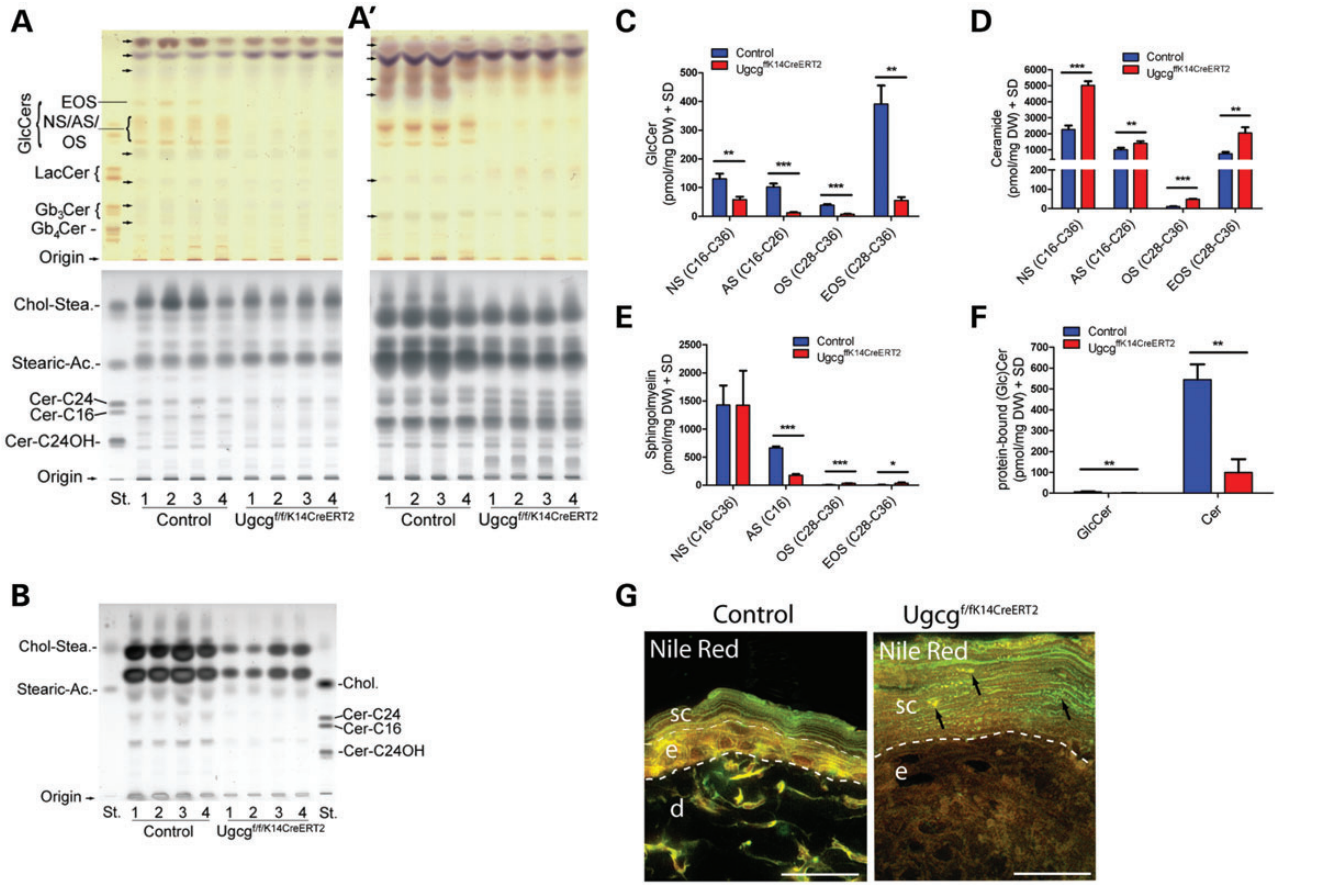

Figure 2. Epidermal lipid analysis and organization. The epidermal SL composition in control and mutant skin regarding (**A**, **A′**) free extractable and (**B**) protein-bound SLs was investigated by thin-layer chromatography (TLC) and quantified by MS (**C**–**F**). (A, A′, top) Orcinol staining of GSLs in (A) crude extracts and (A′) after alkaline treatment revealed a significant reduction of glucosylceramides (GlcCers), the by-far most prominent GSLs in the epidermis. (A, A′, bottom) Copper staining of free extractable ceramides (Cers) showed quantitative differences in the Cer-pattern of *Ugcg*$^{f/f/K14CreERT2}$ and controls. (B) Protein-bound Cers were drastically reduced in Ugcg-deficient epidermis. TLC results were corroborated by quantitative MS analysis (**C**–**F**) and proofed that all GlcCers (C; NS, AS, (E)OS) and protein-bound species (F) were significantly reduced in *Ugcg*-mutant epidermis, whereas free extractable Cers (D), significantly increased in mutant tissue as compared to controls. (E) Within the sphingomyelins (SMs), non-hydroxy fatty acid (FA)-containing SMs (NS, C16 to C30) appeared unaltered whereas ω-hydroxylated ULC FA-containing SMs (OS and EOS) increased. Surprisingly, C16 α-hydroxylated fatty acid-containing species (AS) drastically decreased. (**G**) Alterations in the lipid constitution were reflected by an abnormal lipid lamellar structure of mutant stratum corneum (SC). Lentil-like lipid aggregates within the lamellae of corneocytes were seen by Nile Red staining. (E)OS, (esterified) ω-hydroxylated FA-containing Cers; NS, non-hydroxy FA-containing Cers; AS, α-hydroxy FA-containing Cers; $^{*}P < 0.05$; $^{**}P < 0.01$; $^{***}P < 0.001$; $n = 4$; mean values ± SD are shown.

by a scaffold of these proteins (IVL-EVPL, LOR-SPRRPs) which form ester bonds to ωh ULC-FAs from Cers, generating an insoluble rigid CE as the first barrier against water loss (6,14).

Keratohyalin granules (KGs) of the SG contain large F-granules (profilaggrin (proFLG)) and small L-granules (LOR). These granules are storage vesicles for major corneocyte and CE proteins. In controls, proFLG and filaggrin (FLG) were normally located in the outer SG and SC, whereas in mutant epidermis F-granules were present in almost all suprabasal layers showing highest intensity in the SC (Fig. 6B). KGs were more numerous and larger in size throughout SS and SG layers of mutant epidermis when compared with controls, suggesting a defect in (pro)FLG synthesis and processing. Immunoblots supported these results: monomeric (1 FLG) and dimeric Flg (2 FLG) as well as polymeric Flg (FLG2) were reduced, whereas other proFLG peptides of abnormal chain lengths accumulated in mutant epidermis (Fig. 6A). During early CE assembly, IVL shifts from the cytosol to be aligned along the plasma membrane of keratinocytes. At the SG/SC interface, this membrane gets gradually replaced by a CE, indicated in control epidermis by the polarized staining pattern of IVL (Fig. 6C). Instead, the latter was strongly expressed in the cytosol of late SS and SG KCs (Fig. 6C), indicating a delay in IVL processing when compared with controls. Western blotting supported these results revealing a reduced protein level of IVL (Fig. 6A). LOR is the major compound of the CE (80–85% of total CE weight) and initially expressed late during CE formation. In control skin, LOR expression appeared late at the SG/SC interface, whereas mutants displayed an earlier strong cytosolic as well as diffuse nuclear staining (Fig. 6D), indicating a mislocalization and delay in LOR processing. Western blot results evidenced a reduction in LOR expression in mutant epidermis (Fig. 6A). The disarray in terminal KC differentiation (into anuclear corneocytes) was additionally apparent by the detection of nuclei (DAPI staining) in SC KCs (Fig. 6B–D; white arrows).

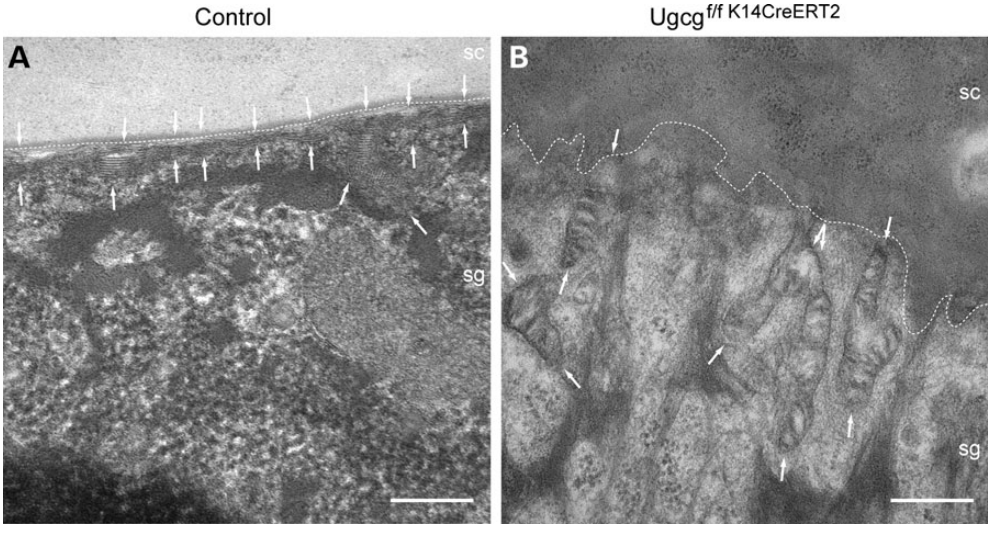

Figure 3. Transmission electron micrographs of ventral skin sections. Lamellar bodies and lipid lamellae showed a regular shape in cells of the *stratum granulosum* from control mice (**A**, arrows). In contrast, LBs in cells of the *stratum granulosum* from mutant mice appeared irregular in shape and with disordered lamellar arrangement (**B**, arrows). Dotted lines indicate the border between *stratum granulosum* and *stratum corneum*; sc, *stratum corneum*; sg, *stratum granulosum*; scale bars, 200 nm.

Wound healing of full thickness skin wounds is delayed in GlcCer-depleted skin and skin grafts

Wound healing experiments were performed in control and GlcCer-deficient skin and skin grafts to investigate whether re-epithelialization is affected by the KC differentiation defect. Wound closure of full thickness skin wounds (5 mm in diameter) was significantly delayed at all investigated time points in mutant skin (Fig. 7A and B; Supplementary Material, Fig. S9a–d). Upon wounding, KC proliferation (Supplementary Material, Fig. S9e) as well as dendritic cell and macrophage infiltration were increased in wound sites of *Ugcg*-mutant skin (Supplementary Material, Fig. S9f). Giemsa-positive cells were not different in control and UGCG-deficient skin during the early wound healing phase, whereas on day 6 mast cells remained significantly elevated in mutant skin (Supplementary Material, Fig. S9g). IF staining for keratins of KC differentiation, K14 (early) and K10 (late) revealed that reepithelialization was complete in controls at day nine, whereas wounds in GlcCer-deficient skin were still open and incomplete (Fig. 7C and D). To exclude effects of a systemic factor on the delay in wound closure, transplantation experiments were conducted. Control mice with grafted skin of either wild-type or $Ugcg^{f/fK14CreERT2}$ litters were TAM-induced 5 weeks upon transplantation, when skins were fully adapted and hair growth was observed (Supplementary Material, Fig. S10). Wound healing experiments in isografted skins were performed 3 to 4 weeks upon TAM induction and had a similar outcome regarding K14 and K10 expression at day 9 of healing (Fig. 7E and F) as reported for control and $Ugcg^{f/fK14CreERT2}$ mice.

Gene expression analysis reveals alterations of genes involved in lipid homeostasis and KC development

In order to identify differentially expressed genes and enriched molecular networks resulting from epidermal *Ugcg* gene deletion, we conducted gene expression profiling and subsequent gene ontology (GO) enrichment analyses. Using the Genomatix single-probe approach, a total set of 362 differentially regulated transcripts was found from which 168 were induced and 194 were suppressed in the mutant epidermis (FDR = 0).

As described, UGCG-deficient mice showed alterations in epidermal lipid composition and KC differentiation. GO-enrichment of altered genes disclosed related processes such as lipid metabolism (GO:0006629, GO:0008610, GO:0044255) and epidermal differentiation processes (GO:0008544, GO:0031424, GO:0009611, GO:050678) (Supplementary Material, Table S5). Differentially expressed genes corresponding to these specific GO terms are illustrated in Figure 8A and B.

Genes encoding for enzymes involved in lipid metabolism were found to be induced on the mRNA level. A subset of these enzymes is particularly involved in the SL pathway promoting Cer synthesis such as (i) desaturase 2 (*Degs2*, FC 3.5), which catalyzes Cer formation from dihydroceramide, (ii) neutral sphingomyelinase (*Smpd3*, FC 2.5), which catalyzes Cer formation from plasma-membrane derived SM (lysosomal acidic sphingomyelinase was not affected), (iii) sphingosine-1-phosphate phosphatase 2 (*Sgpp2*, FC 2.6), which generates Sph from Sph-1-P, and (iv) CerS3 (encoded by the gene *Lass3*, FC 1.7), which catalyzes the synthesis of ceramides (Fig. 8A and C). These results indicate an increase in Cer formation in *Ugcg*-mutant skin which is in line with the results obtained by MS.

Furthermore, mRNA and protein levels of the transcriptional activators peroxisome proliferator-activated receptor β/δ (PPARβ/δ) and fatty acid binding protein 5 (FABP5) were detected to be significantly induced (FC 1.8 and FC 2.1, respectively) (Fig. 8A, B, D). Both have been reported in regulating lipid transport, lipid signaling and differentiation in KCs (22–25). Moreover, mRNA levels of potential PPARβ/δ target genes involved in proliferation and cell survival were significantly enhanced, e.g. members of the EGF family such as epigen (*Epgn*, FC 3.3) and heparin-binding EGF-like growth factor (*Hbegf*, FC 2.5) as well as lipid chaperones such as retinol binding protein 2 (*Rbp2*, FC 3.1), *Fabp5* (FC 2.1) and cellular retinoic acid-binding protein 2 (*Crabp2*, FC 1.7).

To summarize, the identified gene subsets corroborate the observed phenotypes resulting from *Ugcg* gene deletion at the

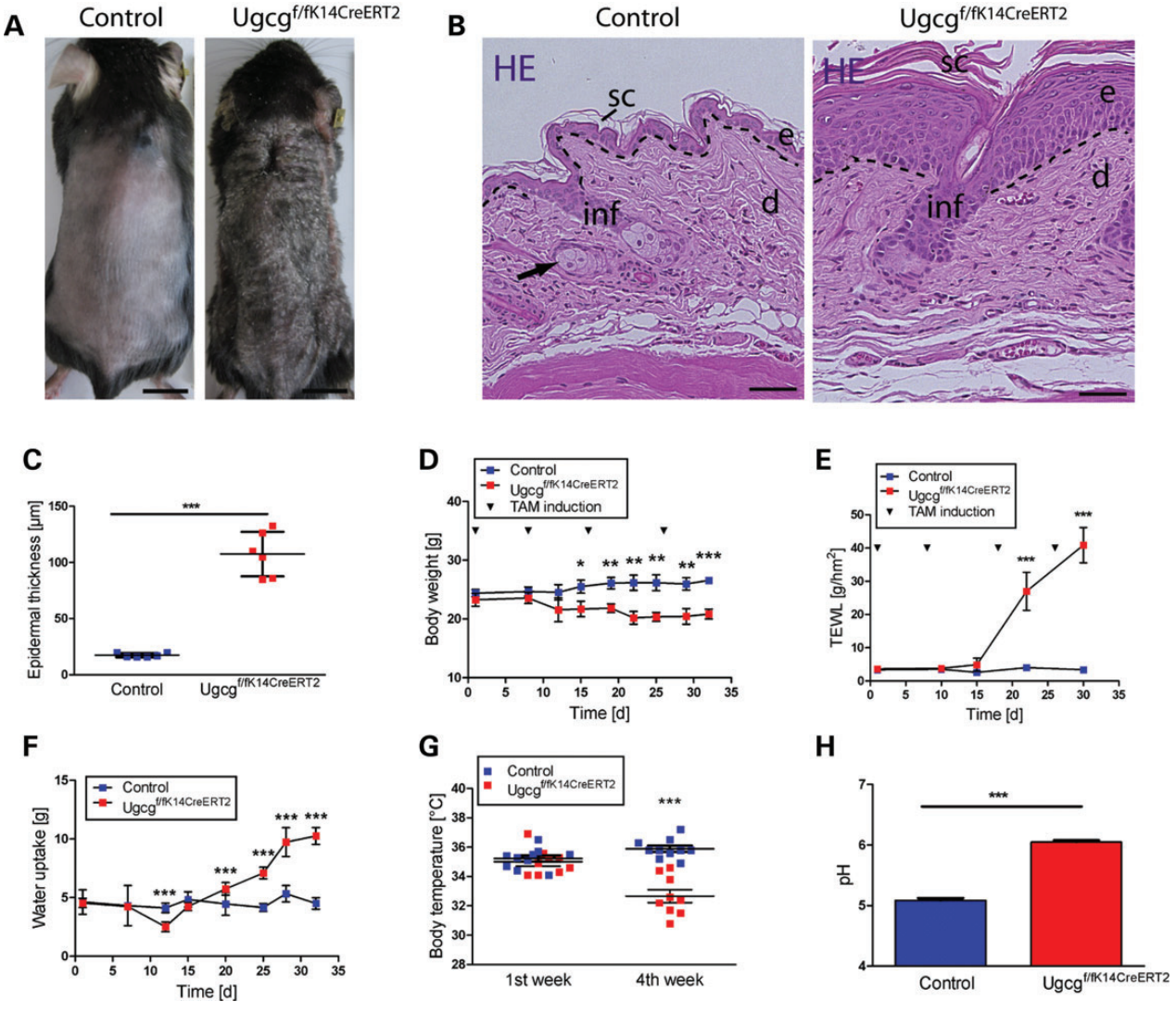

Figure 4. Phenotypical analysis of control- and *Ugcg*$^{f/fK14CreERT2}$ mice. (**A**) *Ugcg*-mutant mice showed dry, scaling skin, greasy fur and impaired hair growth 3 weeks upon TAM induction. (**B**) HE staining revealed hyperstratifed epidermis in mutants with a 5-fold increase in epidermal thickness in the fourth week after induction (**C**). (**D**) Body weight of *Ugcg*$^{f/fK14CreERT2}$ mice decreased upon the second induction. In parallel, epidermal barrier failed, as reflected by significant increase of (**E**) TEWL and (**F**) water uptake. (**G**) Body temperature of mutants decreased in the fourth week. (**H**) In addition, the *stratum corneum* pH was significantly elevated in mutants. Dashed lines, dermal/epidermal junction zone; the arrow indicates a sebaceous gland; e, epidermis; d, dermis; inf, infundibulum; sc, *stratum corneum*; scale bars, 0.5 cm (A) and 50 µm (B); $^{*}P < 0.05$; $^{**}P < 0.01$; $^{***}P < 0.001$; mean values ± SD are shown.

molecular level. Furthermore, the results obtained by gene expression profiling (Fig. 8A–C) and western blotting (Fig. 8D) suggest PPARβ/δ and FABP5 as potential transcriptional regulators of epidermal development. Thus, we propose that alterations in Cer homeostasis affect a PPARβ/δ-mediated signaling cascade as one likely mechanism for hyperproliferation in *Ugcg*-mutant epidermis (Fig. 9).

DISCUSSION

Epidermal deficiency of UGCG, the enzyme catalyzing the initial step of GSL biosynthesis, caused early death of constitutive UGCG-deficient (*Ugcg*$^{f/fK14Cre}$) mice, preventing detailed mechanistic insight into the molecular and cellular actions of GlcCers in the epidermis. Inducible *Ugcg*$^{f/fK14CreERT2}$ mice were generated to investigate the role of GlcCers in cell differentiation and epidermal barrier formation. TAM induction of *Ugcg*$^{f/fK14CreERT2}$ mice led to *Ugcg* gene deletion in epidermis as well as in tongue, esophagus and forestomach, where K14-promotor activity had previously been described (26).

Epidermal barrier homeostasis secures optimal protection against environmental stressors and allows for efficient adaptation by the autonomous regulation of epidermal differentiation, cohesion and desquamation. Epidermal barrier function has mainly been attributed to the SC, composed of lipid-embedded corneocytes and a lipid-enriched extracellular matrix (2), as well as to TJ proteins preventing paracellular diffusion and transport (27). Disturbance of one of those factors may lead to severe dermatoses such as ichthyoses, atopic dermatitis and psoriasis (28–31). In our study, UGCG deficiency in skin caused loss of GlcCers, whereas free-extractable Cers (NS, AS, OS, EOS)

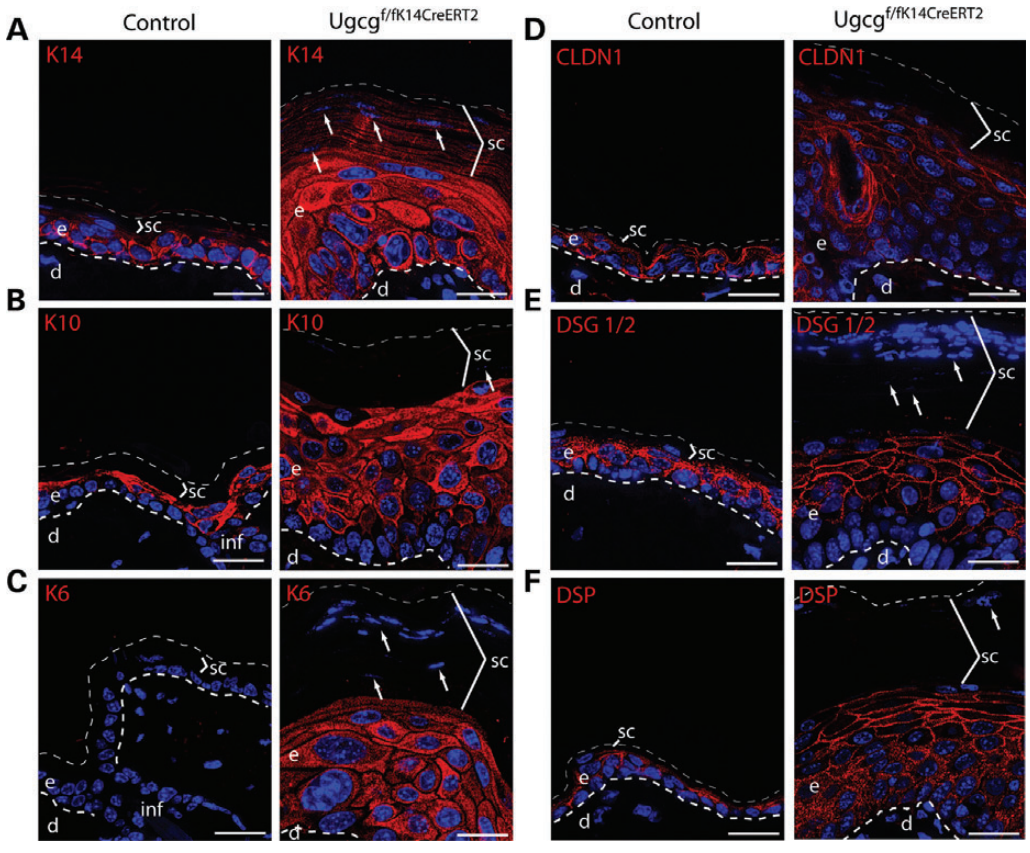

Figure 5. Delayed KC differentiation and junction protein malformation. (**A**) In healthy epidermis, keratin K14 is restricted to the basal layer. *Ugcg*-mutants expressed K14 in all epidermal layers. (**B**) Keratin K10 distribution in the SS appeared regularly, but the number of cell layers was elevated in Ugcg$^{f/fK14CreERT2}$ epidermis. (**C**) Concomitantly with the observed hyperkeratosis, stress-induced keratin K6 was detected in mutant epidermis. Junction protein expression (**D**) claudin 1 (CLDN1) and (**E**) desmogleins 1 and 2 (DSG1/2) in SS/*stratum granulosaum* layers appeared weaker and lost in the *stratum basale* in *Ugcg$^{f/fK14CreERT2}$* epidermis. (**F**) Desmoplakin (DSP) was detected as typical granular staining in the mutant epidermis. Note the nuclear remnants present in the *stratum corneum* layers of UGCG-deficient skin, reflecting the delay in terminal KC differentiation (A, C, E, F; arrows). e, epidermis; d, dermis; inf, infundibulum; sc, *stratum corneum*; scale bars, 50 μm.

accumulated. However, almost all protein-bound Cers were lost, supporting protein-bound GlcCers as precursors of protein-bound Cers (32). These changes in lipid composition were accompanied by severe ichthyosiform skin abnormalities.

Disruption of the epidermal barrier was evidenced by elevated skin surface pH and water loss; the latter affected temperature regulation in mutant mice. Adult *Ugcg* mutants compensated high water efflux with increased water intake from the onset of barrier loss. In humans, dehydration is a lethal risk factor for infants suffering from congenital harlequin ichthyosis (HI), a severe skin disease based on a gene mutation of the lipid transporter ABCA12, which is important for the shuttling of GlcCers into LBs (33). In these patients, GlcCer accumulation and Cer loss caused similar barrier defects as observed in GlcCer deficiency in our study, underlining the importance of GlcCer-dependent Cer processing for normal barrier function.

The SC of *Ugcg* mutants appeared as a thick rigid layer of partially undifferentiated corneocytes. The disorder in corneocyte maturation was further associated with altered processing of the terminal differentiation markers LOR, and (pro)FLG. Strong cytosolic and nuclear localization of LOR was observed in mutant skin and is a feature of LOR keratoderma, such as Vohwinkel's syndrome (34). Furthermore, FLG depletion is characteristic for atopic skin of patients with *Flg* gene mutations (35,36). Deficient proteolytic cleavage of proFLG was evidenced by western blot, showing diffusive bands of FLG-like intermediates, and reduced levels of polymeric (FLG 2), tri- (3 FLG) and dimeric (2 FLG) FLG precursors. FLG 2 is a 250 kDa FLG polymer, which was found to be reduced in skin of atopic dermatitis patients and in mice fed with essential FA-deficient diet (37), both displaying a similar phenotype as induced *Ugcg$^{f/fK14CreERT2}$* mice. Loss of monomeric FLG might not only hinder keratin condensation in corneocytes (38), but also impair its degradation into water-retaining amino acids (e.g. histidine, glutamine, arginine) and their derivatives (e.g. trans-urocanic acid) within the SC, promoting further dehydration. The latter directly affects an increase in SC pH, which was indeed higher in mutants than in controls. Many enzymes secreted together with the lipids into the SG/SC interface are typically found in the endosomal/lysosomal compartments and have an acidic activity optimum. Elevation of the SC pH impairs activity of such enzymes involved in lipid metabolism (e.g. β-glucocerebrosidase, sphingomyelinases, phospholipases) (39–41) and protein shedding (e.g. kallikreins) (42,43), thereby contributing to hypercornification and disturbed barrier function.

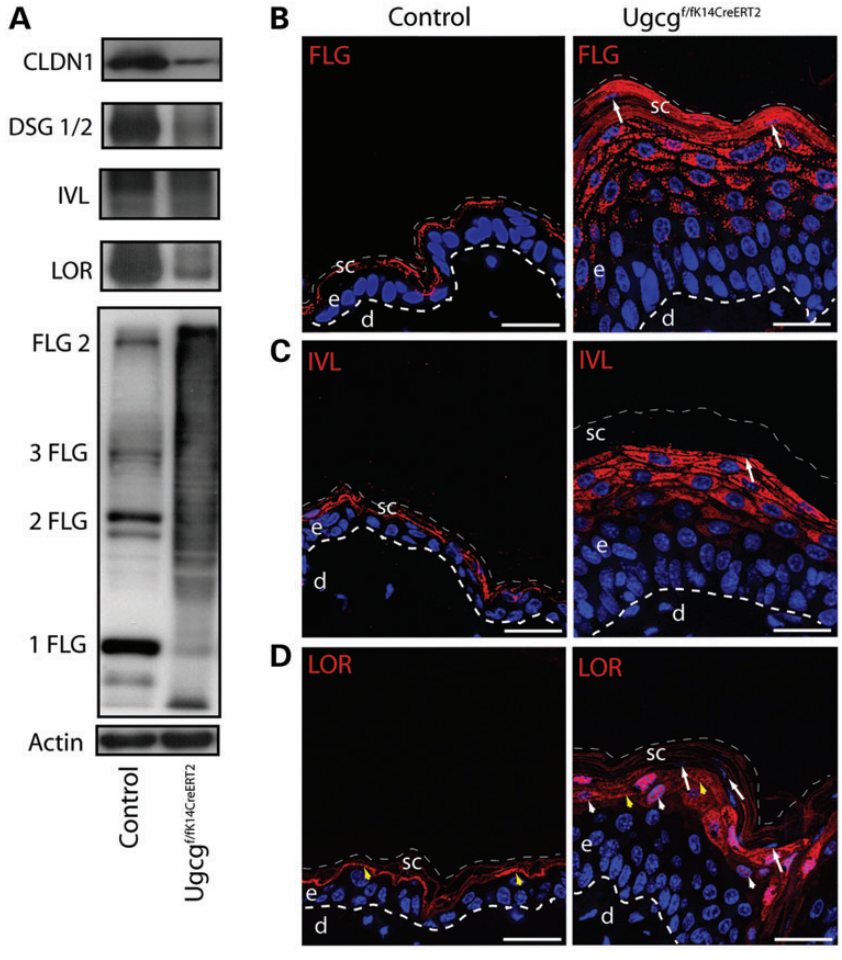

Figure 6. Impaired cornification and CE formation. (**A**) Western blot analysis confirmed a deficit in protein expression or impaired processing of claudin 1 (CLDN1), desmoglein 1 and 2 (DSG1/2), IVL, LOR and filaggrin (FLG) in mutant epidermis. (**B**) IF microscopy of the terminal differentiation protein FLG showed a strong dotted-like pattern in the upper epidermal layers of mutant skin. (**C**) IVL was early expressed in the late SS cells in mutants and showed a more cytosolic staining pattern when compared with controls. (**D**) Cornified envelope (CE) marker LOR was expressed in the *stratum granulosum* and *stratum corneum* (SC) in mutants. Its staining alternated throughout the granular layer, but clearly encircled the rim of f-granules in control and mutant skin (yellow arrowheads). Note the nuclear remnants in mutant SC (A, B; white arrows). Dashed lines indicate the dermal/epidermal junction zone and the apical margin of the SC respectively. e, epidermis; d, dermis; sc, *stratum corneum;* scale bars, 50 μm.

Epidermis devoid of GSLs showed severe hyperkeratosis and loss of the WPB. GlcCer-depleted skin of adult mutants had a drastic reduction in protein-bound Cers which was in contrast to newborn constitutive *Ugcg*$^{f/fK14Cre}$ mice, in which protein-bound Cers were not altered at P5 yet (18). Newborn mice died before one cycle of epidermal turnover was completed, explaining the discrepancy between the constitutive and inducible *Ugcg* deficiency model. Loss of protein-bound Cers upon UGCG depletion in adult mice, however, supports protein-bound GlcCers as their metabolic precursors. Nevertheless, EOS-Cers were not lost in GlcCer-deficient skin, but instead accumulated, indicating no direct involvement of UGCG for their biosynthesis. The loss of GlcCers in *Ugcg*$^{f/fK14CreERT2}$ mice resulted in a significant increase in corresponding Cers (OS and EOS) when compared with controls. These results show that GlcCers serve as essential intermediates, carrying and directing Cer transport and processing (18,44).

However, the increase in Cers (by ca. 4500 pmol/mg dry epidermis weight) in *Ugcg* mutants cannot only be accounted for by the loss of GlcCers (by ~670 pmol/mg epidermal dry weight) in these mice. Cer accumulation might result from enhanced Cer *de novo* synthesis at the ER and/or from Cer-recycling in the salvage pathway (conversion of SMs into Cers), as a compensatory mechanism for barrier loss (45,46). Based on enhanced mRNA expression of the membrane-bound neutral sphingomyelinase (*Smpd3*), one may assume an increase in SM recycling leading to increased Cer levels which could also explain the unchanged and even reduced levels of NS- and AS-SMs species, respectively.

Long-chain (LC) and very-long-chain-Cers (C16–C24) can influence the cell fate as evidenced in studies of human cancers and cancer cell lines, showing increased levels of specific NS-Cers (C16, C24, C24:1), promoting apoptosis and tumor progression (47–50). In *Ugcg* mutants, all epidermal NS-Cers significantly accumulated and might be responsible for both increased apoptosis and proliferation of GlcCer-deficient KCs.

Ugcg-deficient mice developed hyperkeratosis indicated by K6 expression and increased numbers of Ki67-positive

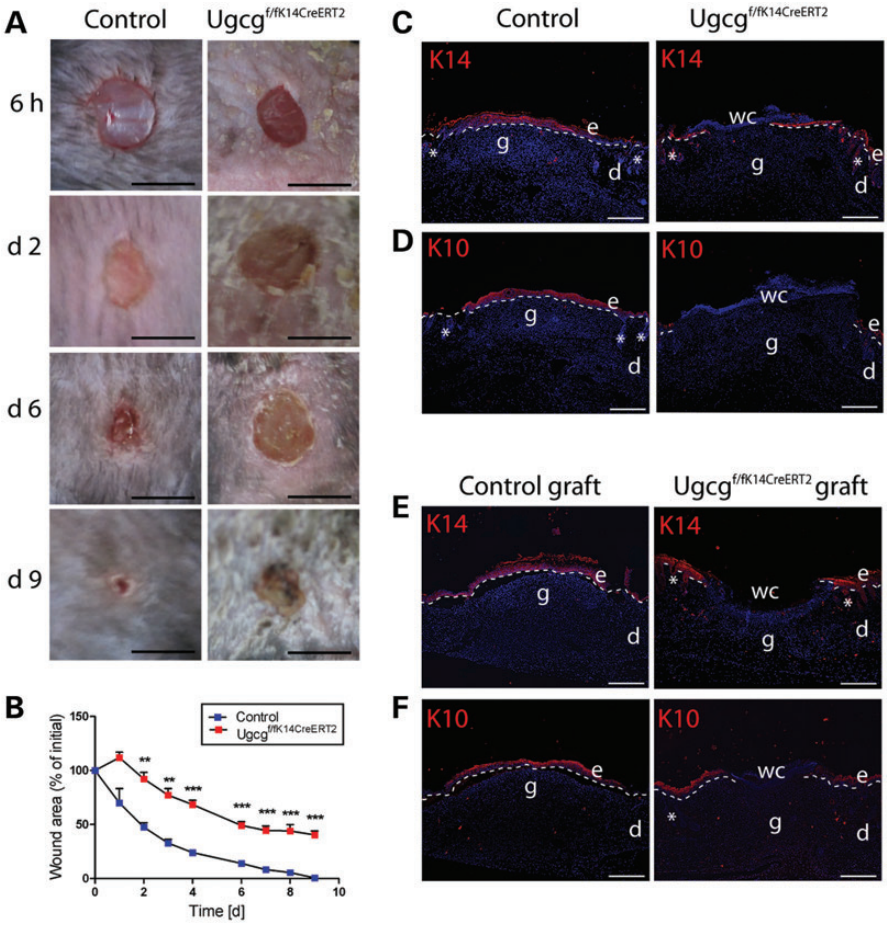

Figure 7. Wound healing is delayed in *Ugcg*$^{f/fK14CreERT2}$ mice. Wounds were monitored (**A**) and wound sizes measured (**B**) at different time points during wound healing (WH). Wound closure was significantly delayed in mutant skin ($n = 3$ each; shown is one representative experiment out of three with similar results). (**C** and **D**) At day 9 of WH, control wounds were fully reepithelialized as demonstrated by keratin 14 (K14) and keratin 10 (K10) staining. In contrast, reepithelialization was significantly delayed in wounds of mutant mice. In transplanted skin from *Ugcg*$^{f/fK14CreERT2}$ mice (**E** and **F**), a similar WH delay as in non-transplanted skin was observed upon TAM induction. d, dermis; e, epidermis; wc, wound center; asterisks indicate hair follicles; scale bars, 0.5 cm (A); 200 μm (C–F).

KCs, including the lower suprabasal layers. Additionally, an epidermis-wide distribution of K14 was noticed, which in control epidermis was restricted to the basal layer. Also cell–cell junction proteins, such as the TJ protein CLDN1 and desmosomal cadherin DSG2, were aberrantly expressed, decreased in the lower layers or (for DSP) widely retained. These alterations were apparently due to an alteration in basal KC differentiation, thereby contributing to delayed wound healing in GlcCer-depleted skin.

Infiltrating macrophages and dendritic cells are normally recruited upon chemotactic stimuli synthesized by KCs (51). Accordingly, GlcCer-depleted KCs themselves might have activated and attracted immune cells as a stress response to impaired epidermal integrity. During wound healing, a tight regulation of the inflammatory phases is important for efficient cutaneous tissue repair, whereas excessive or chronic inflammation can lead to impaired wound healing (e.g. diabetic wounds) (51). Although mutant skin was slightly inflamed at the onset of wounding, the immune response upon wounding was similar to controls and did not alter granulation tissue formation. The lack of K14- and K10-positive cells in wound tissue rather evidenced a defect in reepithelialization as the cause for delayed wound closure. To exclude the possibility of a systemic effect of factors such as water and electrolyte loss as well as low body temperature on wound closure, wound healing experiments were performed in whole skin isografts of control and *Ugcg*$^{f/fK14CreERT2}$ mice upon TAM induction. These experiments corroborated the delay in keratinization in UGCG-deficient skin, thereby excluding systemic effects to play a relevant role. In summary, our results imply that the delay in wound closure was due to a pronounced disturbance of KC differentiation caused by *Ugcg* gene deletion.

Gene expression analysis from *Ugcg* mutant and control skin at day 21 of TAM induction was performed to analyze whether the diseased and hyperproliferative state of the skin would be reflected on the level of gene expression. The genes identified to be differentially expressed at this stage support our findings obtained from lipid, protein and histochemical analysis. Gene expression profiling and enrichment analyses of the molecular events induced upon *Ugcg* gene deletion were partly defined, in particular those affecting SL metabolism and epidermal development. Clustering highlighted genes involved in Cer-synthesis (such as *Lass3*, *Smpd3* and *Degs2*), in Cer-signaling (*Pparβ/δ*) and lipid transport (*Fabp5, Crabp2, Rbp2*) based on the significant increase in Cers in mutant skin and their role as

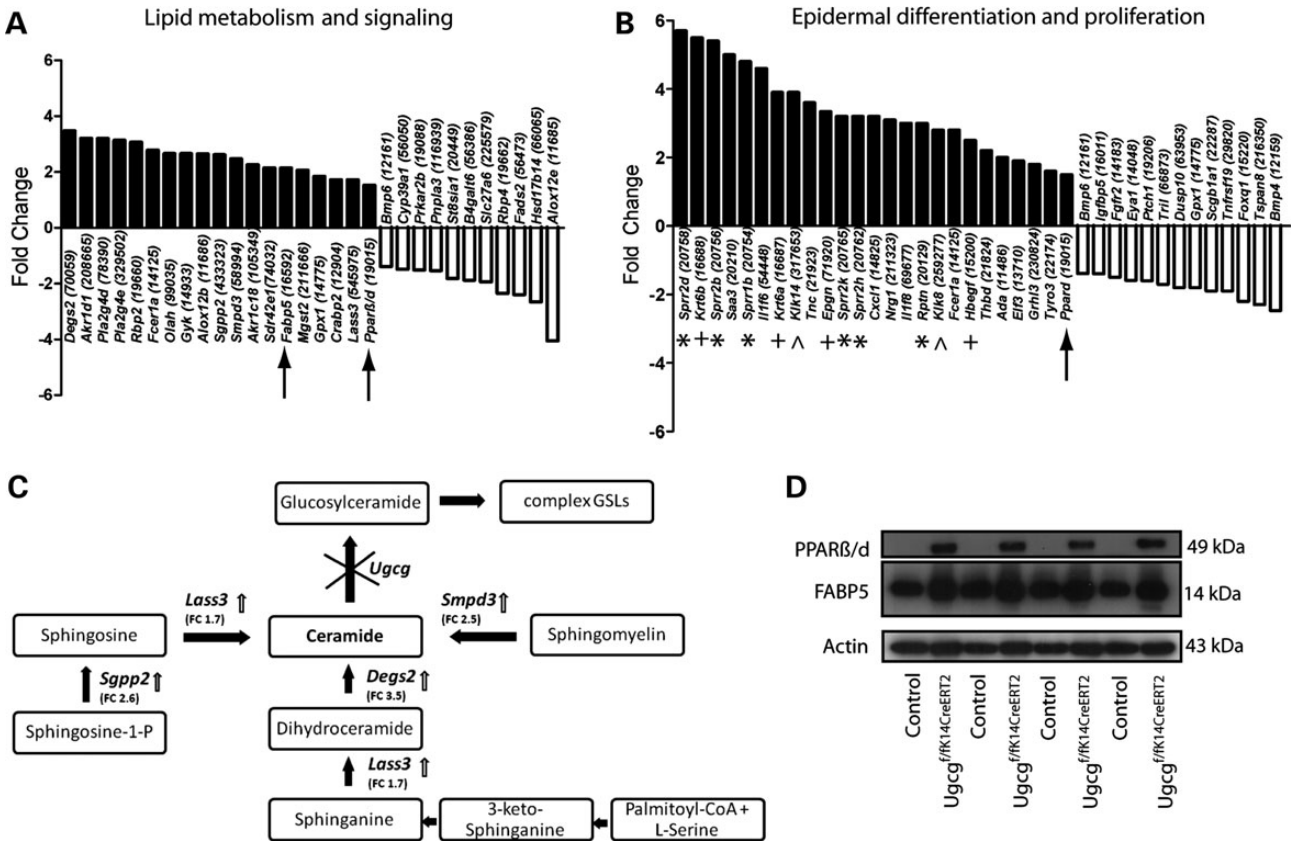

Figure 8. Evaluation of differentially expressed genes in skin of *Ugcg* mutant and control mice. (**B**) Enrichment analysis of differentially expressed genes in GSL-depleted skin revealed prominent induction of genes involved in lipid metabolism and signaling (**A**) as well as in epidermal differentiation/proliferation. (**C**) Gene expression profiling evidenced the upregulation (red arrows) of major Cer-synthesizing enzymes in *Ugcg*-mutant skin. Gene names are: *Lass3*, longevity assurance homolog 3; *Degs2*, desaturase 2; *Smpd3*, neutral sphingomyelinase; *Sgpp2*, sphingosine phosphatase 2; *Ugcg*, glucosylceramide synthase. Numbers in parentheses indicate the fold change (FC). (**D**) Induction of peroxisome proliferator-activated receptor beta/delta (PPARß/δ) and fatty acid binding protein 5 (FABP5) in mutant epidermis was analyzed by western blotting. Numbers in brackets indicate gene IDs (A and B). Arrows mark potential regulators *Pparß/δ* and *Fabp5*; asterisks (*) indicate EDC genes; (+) indicate proliferation related genes, i.e. keratins *K6*, epigen (*Epgn*) and heparin binding EGF-like growth factor (*Hbegf*); (^) indicate kallikreins (*Klk14, Klk8*).

potent activators (NS/AS-Cers) of the nuclear receptor PPARß/δ in KCs (22), mediating cell growth and survival (24). PPARß/δ upregulation, both on the mRNA- as well as the protein-level, might explain the hyperproliferative state of KCs in *Ugcg*-mutant skin, mediated by intracellular accumulating Cers (NS, AS) (48). This was additionally corroborated by enhanced mRNA levels of potential PPARß/δ target genes involved in proliferation and cell survival such as growth factors (e.g. *Epgn*, *Hbegf*) and the lipid chaperone *Fabp5* (24,25). The array and western blot data provide a logic explanation for the observed epidermal hyperproliferation. However, it cannot be excluded that elevated proliferation and delayed keratinocyte differentiation in mutant epidermis had been a consequence of decreased levels of EOS-GlcCers and increased Cer synthesis. EOS-GlcCers have been shown to promote KC maturation enhancing keratinization and CE formation (52–54).

Additionally, gene expression profiling uncovered major alterations in epidermal differentiation complex (EDC) genes such as small proline-rich proteins (*Sprrp's*, FC 3.2–5.7) and repetin (Rptn, FC 3.0) (55). A significant induction was also found for the hyperproliferation markers keratin K6 [*Krt6b* (FC 3.9) and *Krt6a* (FC 5.5)] and the tissue kallikreins *Klk14* (FC 3.9) and *Klk8* (FC 2.8) (Fig. 8B) which belong to the group of secretory serine proteases, involved in the regulation of skin desquamation (56). Upregulation of the EDC genes, keratins K6 and KLKs, has been associated with hyperproliferative/inflammatory skin diseases such as psoriasis and atopic dermatitis (57–59) and additionally reflected the diseased state of GlcCer-depleted skin. A caveat may be considered, when interpreting the gene expression data, that one cannot unequivocally dissect causes and consequences of keratinocyte hyperproliferation by this approach.

We conclude that *Ugcg* deletion led to deficiency of epidermal GlcCers and foremost to an increase of free extractable Cers and ωh-SMs. Sequential Cer-processing was blocked, indicated by drastic reduction of protein-bound Cers. Our data support the idea that Cer-glucosylation is pivotal for a regular transport and ω-esterification of Cers to the CE and a prerequisite for barrier formation by transesterification to corneocyte proteins. GlcCer-depletion in basal KCs affected KC maturation, hampered cornification and wound reepithelialization. Correlates to several human skin diseases can be inferred such as ichthyosis (33,60) and atopic dermatitis (30).

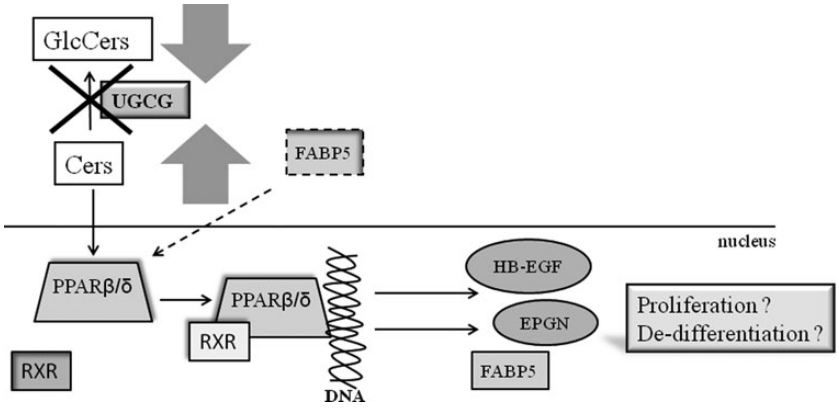

Figure 9. Schematic representation of processes induced upon *Ugcg* deletion and subsequent Cer-accumulation. We hypothesize that elimination of GlcCer synthesis in mutant epidermis leads to Cer accumulation and induction of proliferation and dedifferentiation processes mediated by the peroxisome proliferator-activated receptor β/δ (PPARβ/δ), fatty acid binding protein 5 (FABP5) and potential target genes encoding for proteins such as heparin-binding EGF-like growth factor (HBEGF), epigen (EPGN) and fatty acid binding protein 5 (FABP5) itself.

MATERIALS AND METHODS

Generation of K14CreERT2 knock-in mice

An ∼4.5 kb fragment of the K14-promoter region was amplified by PCR using proof-reading polymerase (PFU, Promega, Heidelberg, Germany). The primers were designed to introduce a *Kpn*I and *Sst*II site at the 5-prime end as well as an ATG start-codon and an *Eco*RV site at the 3-prime end of the PCR product. A second PCR was performed amplifying a ∼4.5 kb fragment including the complete coding sequence of K14 as well as a *Pac*I and *Nhe*I site needed for cloning of the PCR fragment. The correctness of both PCR products was proven by sequence analysis. The 5-prime homology arm was inserted via *Kpn*I/*Eco*RV in frame into a modified cloning vector containing an iCre-, an ERT2- and a FRT-flanked neomycin selection cassette (Supplementary Material, Fig. S1a). The 3-prime homology arm was inserted into *Pac*I/*Nhe*I at the 3-prime end of the neomycin cassette. The targeting construct was then ligated via *Sst*II/*Cla*I into a cloning vector containing a PGK-DTA cassette (Supplementary Material, Fig. S1a) in order to enhance the efficiency of the homologous recombination in embryonic stem (ES) cells. E14 ES cells were transfected in the presence of the *Sst*II-linearized K14-targeting vector and cultivated and genotyped as described (61). As revealed by southern blot analysis using digoxigenin-labeled probes, 4 out of 384 ES cell clones were correctly targeted (Supplementary Material, Fig. S1b and S1c). Positive stem cells were injected into blastocysts and resulting chimeras were mated with C57Bl6 mice. Germ-line transmission was indicated by agouti-like color of the fur from the offspring which were additionally genotyped by southern blot analysis (Supplementary Material, Fig. S1d) and PCR (Supplementary Material, Fig. S1e and S1f). The neomycin selection cassette of the targeted allele was removed by crossing *K14CreERT2-neo* mice with FLP-deleter mice (kindly provided by G. Schütz, DKFZ-Heidelberg) (62). *K14CreERT2* Δ-neo animals were backcrossed for at least five generations until they were combined with floxed *Ugcg* mice of pure C57Bl6 background.

Generation of $Ugcg^{f/fK14CreERT2}$ mice

Homozygous floxed mice ($Ugcg^{f/f}$) were generated as described (61) and crossed with *K14CreERT2* mice. In a second mating step, heterozygous floxed Ugcg Cre mice ($Ugcg^{f/+/K14CreERT2}$) were bred with $Ugcg^{f/f}$ resulting in inducible K14-specific $Ugcg^{f/f/K14CreERT2}$ mice. Heterozygous floxed and $Ugcg^{f/+}$ littermates served as controls. *Ugcg* gene deletion was initiated by intraperitoneal TAM injections each of 1 mg/100 μl oil/injection for four times as indicated in Figure 2D. Controls and $Ugcg^{f/f/K14CreERT2}$ mice were treated in parallel. All animal experiments were approved by federal law (Regierungspräsidium Karlsruhe, Germany).

Southern blot analysis

Biopsies were taken and snap frozen in liquid nitrogen. Epidermis and dermis were separated after trypsinization (0.25% in PBS) of skin for 16 h at 4°C (63) and southern blot analysis was performed as previously reported (18).

Genotyping of mutant mice

Mice were genotyped by PCR and Southern blot analysis as previously described (61) (primers are listed in Supplementary Material, Table S1).

Epidermal lipid extraction and analysis

At the beginning of TAM induction, mice were shaved on the back and hairs were completely removed using depilation cream. Three weeks upon induction, hairless skins were incubated in thermolysin buffer (500 μg/ml) at 37°C for 2 h and epidermis was separated from dermis as previously reported (15). The epidermis was lyophilized, powdered and dry weight was determined. Ten to 50 mg of epidermis was extracted with 2 ml of chloroform/methanol/distilled water (30:60:8 v/v) by volume under sonication at 50°C for 15 min. Extracts were centrifuged at ∼2000*g* for 10 min and supernatants were collected.

Pellets were extracted two additional times as described above using solvent mixtures of chloroform/methanol/distilled water (10:10:1 v/v), and chloroform/methanol (2:1 v/v) by volume and supernatants were pooled with previous fractions. Aliquots of these crude extracts (~10 mg) were further purified by saponification under mild alkaline conditions (0.1 M methanolic KOH, 4 h, 50°C) and desalted using RP-18 columns (Waters Associates, Milford, MA, USA). For extraction of protein-bound SLs, the remaining pellets from the previous extraction steps were first subjected to three cycles of methanol 'washings' to remove remaining free lipids and then saponified under mild alkaline conditions (1 M methanolic KOH, 2 h, 60°C). Supernatants were collected, neutralized with 1 M acetic acid then dried and desalted as previously described in detail (64). Extracted lipids were first analyzed by TLC (64). For analysis of GlcCers, aliquots of saponified and non-saponified crude epidermal extracts corresponding to 1 mg of tissue dry weight were loaded on a HPTLC plate (Silicagel 60 F_{254}, Merck, Darmstadt, Germany). After a pre-run with chloroform/acetone (1:1 v/v), GSLs were separated using chloroform/methanol/water (65:25:4 v/v) as running solvents. Plates were sprayed with 0.2% orcinol in 10% sulfuric acid and developed at 120°C for ~10 min. For the analysis of free-extractable and protein-bound SLs, amounts corresponding to 1 mg of dry epidermis of non-saponified extracts and 0.25 mg of saponified extracts were separated with chloroform/methanol/glacial acetic acid (190:9:1 v/v) as running solvent and sprayed with copper reagent (10% $CuSO_4$ in 8% H_3PO_4) and developed at 180°C for 5–10 min. SLs were further quantified by LC-MS/MS (Xevo TQ-S tandem MS, Waters, Eschborn, Germany) as described (15) (for UPLC-gradient, exact quantitative data and list of determined SL-species, see Supplementary Material, Table S2–S4).

Lipid extraction of the *stratum corneum* (SC)

SC of depilated ventral skin parts was isolated using cyanoacrylate glue-stripping and extracted with n-hexane/CH_3OH 95:5 v/v as described (65,66). The pellet was extracted three times with dimethylformamide at 50°C for 15 min and once with acetone to remove cyanoacrylate. The pellet was dried and solved in 1 M NaOH at 50°C for 5 h. An aliquot of the lysate was used for protein quantification. The amount of Cers was related to the respective total protein content of each sample.

Determination of TEWL and skin surface pH

TEWL was monitored using a Tewameter TM300 (Courage-Khazaka Electronics, Cologne, Germany) as reported (18). SC pH was measured with a *skincheck* pH Meter (PCE, Meschede, Germany).

Determination of body temperature

Body temperature was measured using a rectal thermometer (Almemo (R) 2390-1, sensor: ZA 9040-FS, Ahlborn, Holzkirchen, Germany).

X-Gal staining

LacZ-Rosa26 reporter mice (kindly provided by G. Schütz, DKFZ-Heidelberg) were crossed with K14CreERT2 mice and Cre-activity was monitored in offsprings before and upon TAM induction. Skin cryosections (5 μm) were stained with 5-bromo-4-chloro-3-indolyl-D-galactosidase (X-gal) as previously reported (67,68).

Light microscopy and immunohistochemistry

Skin samples were either formalin fixed (4%) overnight at 4°C, dehydrated and paraffin embedded or frozen in isopentane precooled with liquid nitrogen for cryosectioning. For light microscopy, paraffin sections of 3 μm were deparaffinized and stained by hematoxylin & eosin (HE, Chroma, Köngen, Germany) or with antibodies against HR3 and Ki67 as described (18). Giemsa staining was performed on deparaffinized sections (10 min, RT) using Giemsa azur eosin methylene blue solution (Merck). Then sections were rinsed with 1% acetic acid, sequentially placed in 96% ethanol, 2-propanol (2 × 2 min) and xylol (~1 min) and mounted with Vitro-Clud (Langenbrink, Emmendingen, Germany). For indirect IF microscopy, paraffin sections were subjected to antigen retrieval using 10 mM sodium citrate pH 6 at 96°C for 3–5 min and permeabilization with 0.1% Triton X-100 in PBS at RT for 5 min prior to incubation with primary antibodies at RT for 1 h (Table 1). For the detection of CLDN1, cryosections of 5 μm were fixed in acetone at RT for 10 min followed by incubation with primary antibodies at RT for 1 h (Table 1). Incubation with secondary antibodies was performed at RT for 30 min in parallel with DAPI (20 ng/ml, Sigma) for nuclear staining (Table 2). All stainings were analyzed using a Biorevo Z-9000 fluorescence microscope (Keyence, Neu-Isenburg, Germany).

Electron microscopy

Freshly dissected skin sections were fixed with ruthenium tetroxide solution (Serva, Heidelberg, Germany) and further treated as described (18).

Staining for neutral and phospholipids with Nile Red

Neutral and phospholipids were analyzed as previously reported (69). Cryosections (5 μm) were air-dried, embedded with freshly prepared Nile Red (5 mg/ml in 75% glycerol) and visualized with the fluorescence microscope.

Protein isolation and western blotting

Epidermis and dermis were separated upon incubation in 0.5 M sodium thiocyanate (pH 6.8, in 0.1 M di-sodium hydrogen phosphate) for 30 min on ice as reported (70). Epidermis samples were placed in digitonin lysis buffer and further processed as previously described (15).

Wound healing experiments and isografting

Three weeks upon the start of TAM induction, mice were anesthetized with isoflurane (2.5 vol.%) and a full-thickness

Table 1. Primary antibodies

Antibody	Gene name	Host[a]–clonality[b]	Application[c] (dilution)	Supplier (clone)	Order number
β-Actin	*Actb*	rb–p	WB (1:200)	Santa Cruz	sc-1616-R
Claudin-1	*Cldn1*	rb–p	WB (1:1000) Cryo (1:10)	Thermo Scientific	RB-9209
Desmoglein 1/2	*Dsg 1/2*	m–m	WB (1:100) Paraffin (1:10)	provided by H. Heid (Progen, DG3.10)	–
Desmoplakin	*Dsp*	m–m	WB (1:50) Paraffin (pure)	provided by H. Heid (Progen, DP447)	–
Fatty acid binding protein 5	*Fabp5*	g–p	WB (1:2000)	R&D Systems	AF 1476
(Pro-) Filaggrin	*Flg*	rb–p	WB (1:1000) Paraffin (1:50)	Covance	PRB-417P
HR3	–	r–m	Paraffin (1:50)	Acris, Hiddenhausen, Germany	
Involucrin	*Ivl*	rb–p	WB (1:100) Paraffin (1:100)	Covance	PRB-140C
Keratin K6	*Krt6*	gp–p	Paraffin (1:100)	Provided by L. Langbein	–
Keratin K10	*Krt10*	gp–p	Paraffin (1:100)	Provided by L. Langbein	–
Keratin K14	*Krt14*	gp–p	Paraffin (1:2000)	Provided by L. Langbein	–
Ki67	*MKi67*	r–m	Paraffin (1:200)	Dako (TEC-3)	M7249
Loricrin	*Lor*	rb–p	WB (1:1000) Paraffin (1:100)	Covance	PRB-145P
Peroxisome proliferation-activated receptor δ	*Ppard*	rb–p	WB (1:500)	Thermo Scientific	PA1-823A

[a]g, goat; gp, guinea pig; m, mouse; rb, rabbit; r, rat.
[b]m, monoclonal; p, polyclonal.
[c]Cryo, cryosections; IHC, immunohistochemistry; Paraffin, paraffin sections; WB, western blot.

Table 2. Secondary antibodies

Antibody[a]	Host[a]	Application[b] (dilution)	Supplier (Clone)	Order num.
Alexa FluorR 488 anti-rb	d	IHC (1:500)	Invitrogen	A21206
Alexa FluorR 546 anti-r	g	IHC (1:500)	Invitrogen	A11081
Cy3TM anti-gp	g	IHC (1:500)	Abcam	ab102370
Cy3TM anti-m	d	IHC (1:500)	Jackson Dianova	715-165-150
Cy3TM anti-rb	d	IHC (1:500)	Jackson Dianova	715-165-152
Biotinylated anti-r	rb	Paraffin (1:200)	Vector Laboratories	BA-4001
Goat-HRP	d	WB (1:1000)	Santa Cruz	sc-2020
Mouse-HRP	g	WB (1:1000)	Santa Cruz	sc-2005
Rabbit-HRP	g	WB (1:1000)	Santa Cruz	sc-2004

[a]d, donkey; g, goat; gp, guinea pig; m, mouse; rb, rabbit; r, rat.
[b]IHC, immunohistochemistry; Paraffin, paraffin sections; WB, western blot.

punched biopsy, 5 mm in diameter, was taken from the upper back (using disposable biopsy punches from Stiefel GmbH, Waiblingen, Germany). Wound size, TEWL and body weight of animals were documented over 9–10 days until wounds in control litters were closed. Wounds were collected 6 h, days 2, 6 and 9 upon wounding and fixed in 4% formaldehyde or snap-frozen in liquid nitrogen for immunohistochemistry. Isografting was performed in 7- to 8-week-old male mice (20–25 g). They were anesthetized with tribromoethanol (Avertin, Sigma-Aldrich, Deisenhofen, Germany) and full thickness skin (4 × 4 cm) was excised from donor animals (control and $Ugcg^{f/f/K14CreERT2}$), shortly placed in sterile ice-cold PBS, while skins from acceptor animals (control littermates) were resected. Grafts were sewed on the back of acceptor mice and edges were covered with a semi-permeable dressing (3 M, Neuss, Germany). Transplants were fully adapted within 2–3 weeks upon grafting. TAM induction started 5 weeks upon grafting using the same TAM protocol as described for $Ugcg^{f/fK14CreERT2}$ mice. Wounds were applied in the ninth week upon grafting and monitored until reepithelialization was complete in control mice.

RNA isolation and gene expression profiling

Full thickness skins of $Ugcg^{f/f/K14CreERT2}$ and control mice ($n = 3$, each) were excised using biopsy punches 8 mm in diameter (Stiefel GmbH). RNA was directly extracted (71) and DNase-treated using the Ambion® Turbo DNA-free kit (Life Technologies (Ambion), Darmstadt, Germany). The RNA integrity was validated with the Agilent Bioanalyzer 1000 and 100 ng of total RNA were further processed using the Ambion® WT Expression Kit (Life Technologies (Ambion)) in order to synthesize cDNA, cRNA and finally ss cDNA. The ss cDNA was fragmented and labeled with the WT Terminal Labeling and Controls Kit (Affymetrix, Santa Clara, USA) and hybridized onto GeneChip Mouse Gene 1.0 ST Arrays according to the manufacturer's instructions (Affymetrix). The experiment was performed as independent triplicates. The microarray chips were scanned with a GeneChipTM scanner 3000. Quality control and clustering analyses were carried out using the MADMAX (Management and Analysis Database for Multi-platform microArray eXperiments) platform (https://madmax.bioinformatics.nl, University of Wageningen, Netherlands). For these steps, the CEL files were RMA normalized (72) using the R statistical package (version 2.14.0.) and bioconductor version 2.9. The data were analyzed using Genomatix ChipInspector (for calculating the fold changes) and Genomatix Pathway System (GePS) (Genomatix Software GmbH, München, Germany). These tools

utilize a single probe approach which allows pre-selection of differentially expressed genes. A cut-off of 0% false discovery rate (FDR) was applied to identify significantly regulated genes. Selected genes were further validated by qRT PCR (Supplementary Material, Fig. S11 and Table S6) and western blot (Fig. 8D). All gene expression data are deposited in NCBI's Gene Expression Omnibus (73); (www.ncbi.nlm.nih.gov/geo/; Accession No. GSE47789).

SUPPLEMENTARY MATERIAL

Supplementary Material is available at *HMG* online.

ACKNOWLEDGEMENTS

We thank Martina Volz, Ulrike Rothermel, Sylvia Kaden as well as Gabi Schmidt, Claudia Schmidt, Silke Prätzel-Wunder (German Cancer Research Center, Heidelberg, Germany) and Maria Muciek (Mannheim University, Zentrum für medizinische Forschung (ZMF), Mannheim, Germany) for technical support. We are grateful to Karin Gorgas and Eva Kiss (Heidelberg University, Institute of Anatomy and Cell Biology, Heidelberg, Germany) for critical input to this work.

Conflict of Interest statement. None declared.

FUNDING

This work was supported by the German Research Foundation (SFB 938 to H.-J.G. and SA 1721/2-1 to R.S.) and in parts by the Wilhelm Sander-Stiftung, Munich (Grant 2007.133.2 to L.L.).

REFERENCES

1. Holleran, W.M., Takagi, Y. and Uchida, Y. (2006) Epidermal sphingolipids: metabolism, function, and roles in skin disorders. *FEBS Lett.*, **580**, 5456–5466.
2. Elias, P.M. (2012) Structure and function of the stratum corneum extracellular matrix. *J. Invest. Dermatol.*, **132**, 2131–2133.
3. Kolter, T. and Sandhoff, K. (1999) Sphingolipids—their metabolic pathways and the pathobiochemistry of neurodegenerative diseases. *Angew. Chem. Int.*, **38**, 1532–1568.
4. Sprong, H., Degroote, S., Nilsson, T., Kawakita, M., Ishida, N., van der Sluijs, P. and van Meer, G. (2003) Association of the Golgi UDP-galactose transporter with UDP-galactose:ceramide galactosyltransferase allows UDP-galactose import in the endoplasmic reticulum. *Mol. Biol. Cell*, **14**, 3482–3493.
5. Madison, K.C., Wertz, P.W., Strauss, J.S. and Downing, D.T. (1986) Lipid composition of cultured murine keratinocytes. *J. Invest. Dermatol.*, **87**, 253–259.
6. Sandhoff, R. (2009) Very long chain sphingolipids: tissue expression, function and synthesis. *FEBS Lett.*, **584**, 1907–1913.
7. Doering, T., Proia, R.L. and Sandhoff, K. (1999) Accumulation of protein-bound epidermal glucosylceramides in beta-glucocerebrosidase deficient type 2 Gaucher mice. *FEBS Lett.*, **447**, 167–170.
8. Grayson, S., Johnson-Winegar, A.G., Wintroub, B.U., Isseroff, R.R., Epstein, E.H. Jr and Elias, P.M. (1985) Lamellar body-enriched fractions from neonatal mice: preparative techniques and partial characterization. *J. Invest. Dermatol.*, **85**, 289–294.
9. Vielhaber, G., Pfeiffer, S., Brade, L., Lindner, B., Goldmann, T., Vollmer, E., Hintze, U., Wittern, K.P. and Wepf, R. (2001) Localization of ceramide and glucosylceramide in human epidermis by immunogold electron microscopy. *J. Invest. Dermatol.*, **117**, 1126–1136.
10. Bouwstra, J.A., Honeywell-Nguyen, P.L., Gooris, G.S. and Ponec, M. (2003) Structure of the skin barrier and its modulation by vesicular formulations. *Prog. Lipid Res.*, **42**, 1–36.
11. Madison, K.C. (2003) Barrier function of the skin: 'la raison d'etre' of the epidermis. *J. Invest. Dermatol.*, **121**, 231–241.
12. Marekov, L.N. and Steinert, P.M. (1998) Ceramides are bound to structural proteins of the human foreskin epidermal cornified cell envelope. *J. Biol. Chem.*, **273**, 17763–17770.
13. Doering, T., Holleran, W.M., Potratz, A., Vielhaber, G., Elias, P.M., Suzuki, K. and Sandhoff, K. (1999) Sphingolipid activator proteins are required for epidermal permeability barrier formation. *J. Biol. Chem.*, **274**, 11038–11045.
14. Nemes, Z., Marekov, L.N., Fesus, L. and Steinert, P.M. (1999) A novel function for transglutaminase 1: attachment of long-chain omega-hydroxyceramides to involucrin by ester bond formation. *Proc. Natl Acad. Sci. USA*, **96**, 8402–8407.
15. Jennemann, R., Rabionet, M., Gorgas, K., Epstein, S., Dalpke, A., Rothermel, U., Bayerle, A., van der Hoeven, F., Imgrund, S., Kirsch, J. *et al.* (2012) Loss of ceramide synthase 3 causes lethal skin barrier disruption. *Hum. Mol. Genet.*, **21**, 586–608.
16. Elias, P.M. (1983) Epidermal lipids, barrier function, and desquamation. *J. Invest. Dermatol.*, **80** Suppl, 44s–49s.
17. Hamanaka, S., Hara, M., Nishio, H., Otsuka, F., Suzuki, A. and Uchida, Y. (2002) Human epidermal glucosylceramides are major precursors of stratum corneum ceramides. *J. Invest. Dermatol.*, **119**, 416–423.
18. Jennemann, R., Sandhoff, R., Langbein, L., Kaden, S., Rothermel, U., Gallala, H., Sandhoff, K., Wiegandt, H. and Grone, H.J. (2007) Integrity and barrier function of the epidermis critically depend on glucosylceramide synthesis. *J. Biol. Chem.*, **282**, 3083–3094.
19. Fluhr, J.W. and Elias, P. (2002) Stratum corneum pH: formation and function of the Acid Mantle. *Exog. Dermatol.*, **1**, 163–175.
20. Candi, E., Schmidt, R. and Melino, G. (2005) The cornified envelope: a model of cell death in the skin. *Nat. Rev. Mol. Cell Biol.*, **6**, 328–340.
21. Simpson, C.L., Patel, D.M. and Green, K.J. (2011) Deconstructing the skin: cytoarchitectural determinants of epidermal morphogenesis. *Nat. Rev. Mol. Cell Biol.*, **12**, 565–580.
22. Jiang, Y.J., Uchida, Y., Lu, B., Kim, P., Mao, C., Akiyama, M., Elias, P.M., Holleran, W.M., Grunfeld, C. and Feingold, K.R. (2009) Ceramide stimulates ABCA12 expression via peroxisome proliferator-activated receptor {delta} in human keratinocytes. *J. Biol. Chem.*, **284**, 18942–18952.
23. Kannan-Thulasiraman, P., Seachrist, D.D., Mahabeleshwar, G.H., Jain, M.K. and Noy, N. (2010) Fatty acid-binding protein 5 and PPARbeta/delta are critical mediators of epidermal growth factor receptor-induced carcinoma cell growth. *J. Biol. Chem.*, **285**, 19106–19115.
24. Morgan, E., Kannan-Thulasiraman, P. and Noy, N. (2010) Involvement of fatty acid binding Protein 5 and PPARbeta/delta in prostate cancer cell growth. *PPAR Res.*, doi:10.1155/2010/234629.
25. Han, J., Kioi, M., Chu, W.S., Kasperbauer, J.L., Strome, S.E. and Puri, R.K. (2009) Identification of potential therapeutic targets in human head & neck squamous cell carcinoma. *Head Neck Oncol.*, **1**, 27.
26. Huelsken, J., Vogel, R., Erdmann, B., Cotsarelis, G. and Birchmeier, W. (2001) beta-Catenin controls hair follicle morphogenesis and stem cell differentiation in the skin. *Cell*, **105**, 533–545.
27. Furuse, M., Hata, M., Furuse, K., Yoshida, Y., Haratake, A., Sugitani, Y., Noda, T., Kubo, A. and Tsukita, S. (2002) Claudin-based tight junctions are crucial for the mammalian epidermal barrier: a lesson from claudin-1-deficient mice. *J. Cell Biol.*, **156**, 1099–1111.
28. Radner, F.P., Streith, I.E., Schoiswohl, G., Schweiger, M., Kumari, M., Eichmann, T.O., Rechberger, G., Koefeler, H.C., Eder, S., Schauer, S. *et al.* (2009) Growth retardation, impaired triacylglycerol catabolism, hepatic steatosis, and lethal skin barrier defect in mice lacking comparative gene identification-58 (CGI-58). *J. Biol. Chem.*, **285**, 7300–7311.
29. Scharschmidt, T.C., Man, M.Q., Hatano, Y., Crumrine, D., Gunathilake, R., Sundberg, J.P., Silva, K.A., Mauro, T.M., Hupe, M., Cho, S. *et al.* (2009) Filaggrin deficiency confers a paracellular barrier abnormality that reduces inflammatory thresholds to irritants and haptens. *J. Allergy Clin. Immunol.*, **124**, 496–506, 506 e491–496.
30. Macheleidt, O., Kaiser, H.W. and Sandhoff, K. (2002) Deficiency of epidermal protein-bound omega-hydroxyceramides in atopic dermatitis. *J. Invest. Dermatol.*, **119**, 166–173.
31. Hong, K.K., Cho, H.R., Ju, W.C., Cho, Y. and Kim, N.I. (2007) A study on altered expression of serine palmitoyltransferase and ceramidase in psoriatic skin lesion. *J. Korean Med. Sci.*, **22**, 862–867.
32. Schuette, C.G., Doering, T., Kolter, T. and Sandhoff, K. (1999) The glycosphingolipidoses—from disease to basic principles of metabolism. *Biol. Chem.*, **380**, 759–766.

33. Zuo, Y., Zhuang, D.Z., Han, R., Isaac, G., Tobin, J.J., McKee, M., Welti, R., Brissette, J.L., Fitzgerald, M.L. and Freeman, M.W. (2008) ABCA12 maintains the epidermal lipid permeability barrier by facilitating formation of ceramide linoleic esters. *J. Biol. Chem.*, **283**, 36624–36635.
34. Ishida-Yamamoto, A., Kato, H., Kiyama, H., Armstrong, D.K., Munro, C.S., Eady, R.A., Nakamura, S., Kinouchi, M., Takahashi, H. and Iizuka, H. (2000) Mutant loricrin is not crosslinked into the cornified cell envelope but is translocated into the nucleus in loricrin keratoderma. *J. Invest. Dermatol.*, **115**, 1088–1094.
35. Palmer, C.N., Irvine, A.D., Terron-Kwiatkowski, A., Zhao, Y., Liao, H., Lee, S.P., Goudie, D.R., Sandilands, A., Campbell, L.E., Smith, F.J. *et al.* (2006) Common loss-of-function variants of the epidermal barrier protein filaggrin are a major predisposing factor for atopic dermatitis. *Nat. Genet.*, **38**, 441–446.
36. Weidinger, S., Illig, T., Baurecht, H., Irvine, A.D., Rodriguez, E., Diaz-Lacava, A., Klopp, N., Wagenpfeil, S., Zhao, Y., Liao, H. *et al.* (2006) Loss-of-function variations within the filaggrin gene predispose for atopic dermatitis with allergic sensitizations. *J. Allergy Clin. Immunol.*, **118**, 214–219.
37. Hansmann, B., Ahrens, K., Wu, Z., Proksch, E., Meyer-Hoffert, U. and Schroder, J.M. (2012) Murine filaggrin-2 is involved in epithelial barrier function and down-regulated in metabolically induced skin barrier dysfunction. *Exp. Dermatol.*, **21**, 271–276.
38. Sandilands, A., Sutherland, C., Irvine, A.D. and McLean, W.H. (2009) Filaggrin in the frontline: role in skin barrier function and disease. *J. Cell Sci.*, **122**, 1285–1294.
39. Holleran, W.M., Takagi, Y., Imokawa, G., Jackson, S., Lee, J.M. and Elias, P.M. (1992) beta-Glucocerebrosidase activity in murine epidermis: characterization and localization in relation to differentiation. *J. Lipid Res.*, **33**, 1201–1209.
40. Schmuth, M., Man, M.Q., Weber, F., Gao, W., Feingold, K.R., Fritsch, P., Elias, P.M. and Holleran, W.M. (2000) Permeability barrier disorder in Niemann-Pick disease: sphingomyelin-ceramide processing required for normal barrier homeostasis. *J. Invest. Dermatol.*, **115**, 459–466.
41. Fluhr, J.W., Kao, J., Jain, M., Ahn, S.K., Feingold, K.R. and Elias, P.M. (2001) Generation of free fatty acids from phospholipids regulates stratum corneum acidification and integrity. *J. Invest. Dermatol.*, **117**, 44–51.
42. Ohman, H. and Vahlquist, A. (1998) The pH gradient over the stratum corneum differs in X-linked recessive and autosomal dominant ichthyosis: a clue to the molecular origin of the 'acid skin mantle'? *J. Invest. Dermatol.*, **111**, 674–677.
43. Lin, T.K., Crumrine, D., Ackerman, L.D., Santiago, J.L., Roelandt, T., Uchida, Y., Hupe, M., Fabrias, G., Abad, J.L., Rice, R.H. *et al.* (2012) Cellular changes that accompany shedding of human corneocytes. *J. Invest. Dermatol.*, **132**, 2430–2439.
44. Chujor, C.S., Feingold, K.R., Elias, P.M. and Holleran, W.M. (1998) Glucosylceramide synthase activity in murine epidermis: quantitation, localization, regulation, and requirement for barrier homeostasis. *J. Lipid Res.*, **39**, 277–285.
45. Grubauer, G., Feingold, K.R. and Elias, P.M. (1987) Relationship of epidermal lipogenesis to cutaneous barrier function. *J. Lipid Res.*, **28**, 746–752.
46. Geilen, C.C., Wieder, T. and Orfanos, C.E. (1997) Ceramide signalling: regulatory role in cell proliferation, differentiation and apoptosis in human epidermis. *Arch. Dermatol. Res.*, **289**, 559–566.
47. Schiffmann, S., Sandner, J., Birod, K., Wobst, I., Angioni, C., Ruckhaberle, E., Kaufmann, M., Ackermann, H., Lotsch, J., Schmidt, H. *et al.* (2009) Ceramide synthases and ceramide levels are increased in breast cancer tissue. *Carcinogenesis*, **30**, 745–752.
48. Hartmann, D., Lucks, J., Fuchs, S., Schiffmann, S., Schreiber, Y., Ferreiros, N., Merkens, J., Marschalek, R., Geisslinger, G. and Grosch, S. (2012) Long chain ceramides and very long chain ceramides have opposite effects on human breast and colon cancer cell growth. *Int. J. Biochem. Cell Biol.*, **44**, 620–628.
49. Koybasi, S., Senkal, C.E., Sundararaj, K., Spassieva, S., Bielawski, J., Osta, W., Day, T.A., Jiang, J.C., Jazwinski, S.M., Hannun, Y.A. *et al.* (2004) Defects in cell growth regulation by C18:0-ceramide and longevity assurance gene 1 in human head and neck squamous cell carcinomas. *J. Biol. Chem.*, **279**, 44311–44319.
50. Eto, M., Bennouna, J., Hunter, O.C., Lotze, M.T. and Amoscato, A.A. (2006) Importance of C16 ceramide accumulation during apoptosis in prostate cancer cells. *Int. J. Urol.*, **13**, 148–156.
51. Eming, S.A., Krieg, T. and Davidson, J.M. (2007) Inflammation in wound repair: molecular and cellular mechanisms. *J. Invest. Dermatol.*, **127**, 514–525.
52. Uchida, Y., Hamanaka, S., Matsuda, K., Mimura, K. and Otsuka, F. (1996) Effect of a chemically-synthesized acylglucosylceramide, epidermoside, on normal human keratinocyte differentiation. *J. Dermatol. Sci.*, **12**, 64–68.
53. Uchida, Y., Iwamori, M. and Nagai, Y. (1990) Activation of keratinization of keratinocytes from fetal rat skin with N-(O-linoleoyl) omega-hydroxy fatty acyl sphingosyl glucose (lipokeratinogenoside) as a marker of epidermis. *Biochem. Biophys. Res. Commun.*, **170**, 162–168.
54. Uchida, Y., Ogawa, T., Iwamori, M. and Nagai, Y. (1991) Enhancement of keratin synthesis induced by lipokeratinogenoside, N-(O-linoleoyl)-omega-hydroxy fatty acyl sphingosyl glucose, in association with alteration of the intracellular Ca(2+)-content and protein kinase in cultured keratinocytes (FRSK). *J. Biochem.*, **109**, 462–465.
55. Kypriotou, M., Huber, M. and Hohl, D. (2012) The human epidermal differentiation complex: cornified envelope precursors, S100 proteins and the 'fused genes' family. *Exp. Dermatol.*, **21**, 643–649.
56. Cork, M.J., Danby, S.G., Vasilopoulos, Y., Hadgraft, J., Lane, M.E., Moustafa, M., Guy, R.H., Macgowan, A.L., Tazi-Ahnini, R. and Ward, S.J. (2009) Epidermal barrier dysfunction in atopic dermatitis. *J. Invest. Dermatol.*, **129**, 1892–1908.
57. Bergboer, J.G., Tjabringa, G.S., Kamsteeg, M., van Vlijmen-Willems, I.M., Rodijk-Olthuis, D., Jansen, P.A., Thuret, J.Y., Narita, M., Ishida-Yamamoto, A., Zeeuwen, P.L. *et al.* (2011) Psoriasis risk genes of the late cornified envelope-3 group are distinctly expressed compared with genes of other LCE groups. *Am. J. Pathol.*, **178**, 1470–1477.
58. Iizuka, H., Takahashi, H., Honma, M. and Ishida-Yamamoto, A. (2004) Unique keratinization process in psoriasis: late differentiation markers are abolished because of the premature cell death. *J. Dermatol.*, **31**, 271–276.
59. Komatsu, N., Saijoh, K., Kuk, C., Liu, A.C., Khan, S., Shirasaki, F., Takehara, K. and Diamandis, E.P. (2007) Human tissue kallikrein expression in the stratum corneum and serum of atopic dermatitis patients. *Exp. Dermatol.*, **16**, 513–519.
60. Akiyama, M., Sugiyama-Nakagiri, Y., Sakai, K., McMillan, J.R., Goto, M., Arita, K., Tsuji-Abe, Y., Tabata, N., Matsuoka, K., Sasaki, R. *et al.* (2005) Mutations in lipid transporter ABCA12 in harlequin ichthyosis and functional recovery by corrective gene transfer. *J. Clin. Invest.*, **115**, 1777–1784.
61. Jennemann, R., Sandhoff, R., Wang, S., Kiss, E., Gretz, N., Zuliani, C., Martin-Villalba, A., Jager, R., Schorle, H., Kenzelmann, M. *et al.* (2005) Cell-specific deletion of glucosylceramide synthase in brain leads to severe neural defects after birth. *Proc. Natl Acad. Sci. USA*, **102**, 12459–12464.
62. Rodriguez, C.I., Buchholz, F., Galloway, J., Sequerra, R., Kasper, J., Ayala, R., Stewart, A.F. and Dymecki, S.M. (2000) High-efficiency deleter mice show that FLPe is an alternative to Cre-loxP. *Nat. Genet.*, **25**, 139–140.
63. Mertens, A.E., Rygiel, T.P., Olivo, C., van der Kammen, R. and Collard, J.G. (2005) The Rac activator Tiam1 controls tight junction biogenesis in keratinocytes through binding to and activation of the Par polarity complex. *J. Cell Biol.*, **170**, 1029–1037.
64. Jennemann, R., Kaden, S., Sandhoff, R., Nordstrom, V., Wang, S., Volz, M., Robine, S., Amen, N., Rothermel, U., Wiegandt, H. *et al.* (2012) Glycosphingolipids are essential for intestinal endocytic function. *J. Biol. Chem.*, **287**, 32598–32616.
65. Imokawa, G., Abe, A., Jin, K., Higaki, Y., Kawashima, M. and Hidano, A. (1991) Decreased level of ceramides in stratum corneum of atopic dermatitis: an etiologic factor in atopic dry skin? *J. Invest. Dermatol.*, **96**, 523–526.
66. Takagi, Y., Kriehuber, E., Imokawa, G., Elias, P.M. and Holleran, W.M. (1999) Beta-glucocerebrosidase activity in mammalian stratum corneum. *J. Lipid. Res.*, **40**, 861–869.
67. Soriano, P. (1999) Generalized lacZ expression with the ROSA26 Cre reporter strain. *Nat. Genet.*, **21**, 70–71.
68. el Marjou, F., Janssen, K.P., Chang, B.H., Li, M., Hindie, V., Chan, L., Louvard, D., Chambon, P., Metzger, D. and Robine, S. (2004) Tissue-specific and inducible Cre-mediated recombination in the gut epithelium. *Genesis*, **39**, 186–193.
69. Greenspan, P., Mayer, E.P. and Fowler, S.D. (1985) Nile red: a selective fluorescent stain for intracellular lipid droplets. *J. Cell Biol.*, **100**, 965–973.
70. Diaz, L.A., Heaphy, M.R., Calvanico, N.J., Tomasi, T.B. and Jordon, R.E. (1977) Separation of epidermis from dermis with sodium thiocyanate. *J. Invest. Dermatol.*, **68**, 36–38.

71. Chomczynski, P. and Sacchi, N. (2006) The single-step method of RNA isolation by acid guanidinium thiocyanate-phenol-chloroform extraction: twenty-something years on. *Nat. Protoc.*, **1**, 581–585.
72. Irizarry, R.A., Hobbs, B., Collin, F., Beazer-Barclay, Y.D., Antonellis, K.J., Scherf, U. and Speed, T.P. (2003) Exploration, normalization, and summaries of high density oligonucleotide array probe level data. *Biostatistics*, **4**, 249–264.
73. Edgar, R., Domrachev, M. and Lash, A.E. (2002) Gene Expression Omnibus: NCBI gene expression and hybridization array data repository. *Nucleic Acids Res.*, **30**, 207–210.